Environmental Challenges 3 (2021) 100058

Contents lists available at ScienceDirect

Environmental Challenges

journal homepage: www.elsevier.com/locate/envc

Immobilised tannin: Efficient trap for nickel and lead ions in aqueous solution

Patience M. Shilowa[a], Bamidele J. Okoli[a,c,*], Olugbemi T. Olaniyan[d], Johannes S. Modise[b], Fanyana Mtunzi[a]

[a] Institute of Chemical and Biotechnology, Vaal University of Technology, Southern Gauteng Science and Technology Park, Private Bag X021, Vanderbijlpark 1911, South Africa
[b] Department of Chemistry, Vaal University of Technology, Southern Gauteng Science and Technology Park, Private Bag X021, Vanderbijlpark 1911, South Africa
[c] Department of Chemical Sciences, Faculty of Science and Technology, Bingham University, PMB 005, Karu, Nasarawa State, Nigeria
[d] Laboratory for Reproductive Biology and Developmental Programming, Department of Physiology, Edo University Iyamho, Edo State, Nigeria

ARTICLE INFO

Keywords:
Acacia mearnsii
Adsorption
Pollutant
Heavy metal
Tannin resin
Iron doped-tannin resin

ABSTRACT

Quantity of water is a major concern, but the quality is of more urgent concern due to heavy metal pollution. In this study, the focus was to develop adsorbents (tannin resin (TR) and iron-doped tannin resin (Fe-TR)) from invasive *Acacia mearnsii* for Pb^{2+} and Ni^{2+} in solution. The developed TR and Fe-TR were prepared directly by crosslinking and iron-grafting; respectively with thermal stable at ≤ 350 °C. Surface functionality analysis revealed the presence of chelating groups at ≈ 1688 and 3661 cm^{-1}. The crystallite sizes of the adsorbents were smaller compared to tannin; however, the % carbon and nitrogen were significantly higher. Also, the Brunauer–Emmet–Teller study revealed that iron-grafting of tannin after crosslinking increases the surface area, pore volume and pore size. Furthermore, the surface morphology of adsorbents indicated a well-defined structure with the formation of a whitish deposit and rough lump-like after ion uptake. Both adsorbents showed a type II isotherm with adsorption capacities of 40.650 mg/g and 13.763 mg/g for Pb^{2+} and 120.63 mg/g and 110.74 for Ni^{2+} ion by TR and Fe-TR; respectively. The absorbate-adsorbent interactions were observed to be endothermic with negative and positive Gibb's free energy values for the adsorption of Pb^{2+} and Ni^{2+}; respectively. The adsorption kinetics of Ni^{2+} is governed by several models; however, Pb^{2+} interaction is regulated by Pseudo-second-order model. Furthermore, the data generated offered the possibility of both chemisorption and physisorption processes; highlighting the flexibility and multifunctionality of tannin traps for the erasure of ion impurities in wastewater.

1. Introduction

Water pollution is currently a global concern, in South Africa, there is currently limited quality water due to industrial waste, strip mining, thalassic dumping, oil leaks, fertilizers, acaricides, destruction of river catchments, sewage and wastewater (Otieno and Ochieng, 2004; Valavanidis and Vlachogianni, 2010; Wasi et al., 2013). One of the most toxic water pollutants is heavy metals; adjudged as a major water pollutant due to their effect on ecosystems (Govind and Madhuri, 2014). Heavy metals are toxic chemicals, known to cause multiple organ damage; thus, they are considered a priority toxicant, due to their bio-accumulative and aqua-solubility properties (Stankovic et al., 2014; Verma, 2017). Humans and aquatic life are more exposed to are, lead (Pb) and nickel (Ni), regarded as toxic and human carcinogens through the intake of agricultural products and water (Chowdhury et al., 2016). The primary sources of Pb^{2+} and Ni^{2+} in the environment are waste discharge from industrial sources and mining activities (Liu et al., 2013). Because of their high degree of toxicity, these metals rank amongst the priority metals that are of excessive public health significance.

There are several treatment techniques for removal of Pb^{2+} and Ni^{2+} contaminants in water, which includes physical treatments (such as adsorption, filtration, electrolyte reduction, acoustic cavitation, radiation, and supercritical water oxidation) and chemical treatments (such as reduction with Metals, Fenton's Reagent, TiO_2 photocatalysis and UV/H_2O_2 or Ozone) (Fu and Wang, 2011). Amongst these possible treatments, the adsorption process by solid adsorbents has proven to be the most efficient and low-cost remediation technique for removal of toxic contaminants in water. The task of developing **cost**-effective and efficient materials for the treatment of water remains a daunting task; more so, previous studies were pivoted on plant-based materials, like maize

* Corresponding author at: Institute of Chemical and Biotechnology, Vaal University of Technology, Southern Gauteng Science and Technology Park, Private Bag X021, Vanderbijlpark 1911, South Africa.
E-mail address: okolibj@binghamuni.edu.ng (B.J. Okoli).

https://doi.org/10.1016/j.envc.2021.100058
Received 27 November 2020; Received in revised form 18 February 2021; Accepted 18 February 2021
2667-0100/© 2021 The Author(s). Published by Elsevier B.V. This is an open access article under the CC BY-NC-ND license (http://creativecommons.org/licenses/by-nc-nd/4.0/)

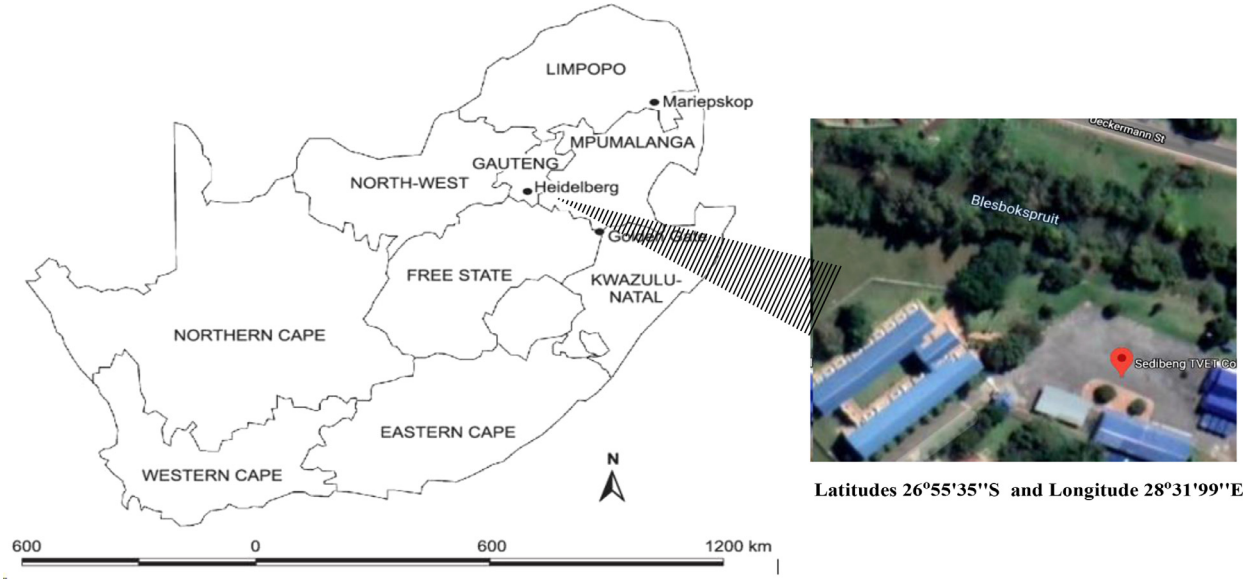


Fig. 1. Geographical location of the *A. mearnsii* sampling site.

leaves and grape stalks (Adesola et al., 2006; Lee et al., 2008. The technically feasible, economical nature, and effective metal removal properties of plant-based adsorbents stand out as major advantages (Xiao et al., 2012).

Review of tannin literature has shown that they are excellent phyto-chelating agents; however, the utilization in water treatment is curbed by its high solubility (Ogata et al., 2011). The usage of tannins in water remediation requires mandatory immobilization of tannins. Our previous studies on invasive *Acacia* spp showed that *Acacia mearnsii* (black wattle) contains a significant amount of tannin; hence, it can be exploited as a tannin feedstock (Joseph and Sekomeng, 2017; Okoli et al., 2018). Using immobilised tannins for the remediation of water will consequentially lead to the application of invasive species to create ecological benefits. We aim is to develop low cost and eco-friendly materials from invasive *A. mearnsii* with water remediation potential; to address the concern of Pb and Ni pollutants in water.

2. Materials and methods

2.1. Chemicals and reagent

Analytical grade chemicals and reagents were used in this investigation. Deionized water was used as a medium in this study.

2.2. Plant collection site and authentication

The samples of *A. mearnsii* (Black wattle) stem bark was collected from Heidelberg, Ratanda (latitude 26°55′35" S and longitude 28°31′99" E) (Fig. 1), Gauteng Province, South Africa. Authentication of the plant was done at the South African National Biodiversity Institute, Pretoria, South Africa, and a voucher number: 17062 was assigned.

2.3. Extraction of tannin and quantification

Collected stem barks were air-dried and milled using a Drotsky S4 Hammermill. According to the method of Ferreira Júnior et al. (2012), tannin was extracted, the resulting menstruum was freeze-dried at −55 °C under vacuum, and stored in a desiccator. According to the Folin-Ciocalteu procedure, the amount of tannin in the extract was estimated and expressed as mg/g of the extract (Naima et al., 2015).

2.4. Cross-linking of tannins

Approximately 48 g of extracted tannin was dissolved at 24 °C in 300 ml of NH_3 solution (13.3 N), 400 mL of benzaldehyde (37 wt%), stirred and filtered. To the residue, 500 mL of distilled water was added and maintained at 70 C for 3 hr. Furthermore, vacuum filtration was carried out followed by stirring and simultaneous addition of 0.1 N HNO_3 (about 100 mL). Thereafter, the mixture was filtered, washed, and allowed to cure at 80 °C before freeze-dried. The solid obtained was then pulverized and sieved to give a 100 μm powdered product tannin resin (TR).

2.5. Iron-grafting of the resin

According to Roto et al. (2016); about 1.5:1 mixture of $FeSO_4{\cdot}7H_2O$ and $FeCl_3{\cdot}6H_2O$ was introduced to 80 mL of hot water followed by 10 min of mechanical stirring. Thereafter, 62 mL of 25% NH_3 solution was introduced followed by 31 g of TR with continuous stirring to give a grey-like insoluble material. The product was washed to a neutral pH with water and labelled iron doped-tannin resin (Fe-TR). Fig. 2 below is a brief summary of the experimental plan.

2.6. Characterisation of adsorbents (TR and Fe-Tr)

2.6.1. Zero surface charge (pH_{pzc}) analysis

Following the protocol reported by Bakatula et al. (2018), the adsorbent points of pH_{pzc} were established by the solid addition procedure. Into various 100 mL conical flasks containing either 0.1 M HCl or NaOH solution; about 50 mL solution of NaCl (0.01 N) with initial pH (2, 4, 6, 8, and 10) was introduced. The initial stabilizing pH readings were noted, followed by the addition of 0.1 g of the adsorbent, stirred at 150 rpm for 2 h; thereafter, the filtered and the final pH of the mixture was documented.

2.7. Batch adsorption experiments

Batch adsorption investigations were conducted to ascertain the influence of initial concentration, pH, temperature, and time on the extraction efficiency of the adsorbents for Pb^{2+} and Ni^{2+} ions.

To a conical flask, approximately 0.5 g and 50 mL of adsorbent and metal ions at a predetermined concentration were added; respectively. After each sorption study, the concentration of the residual metal ion

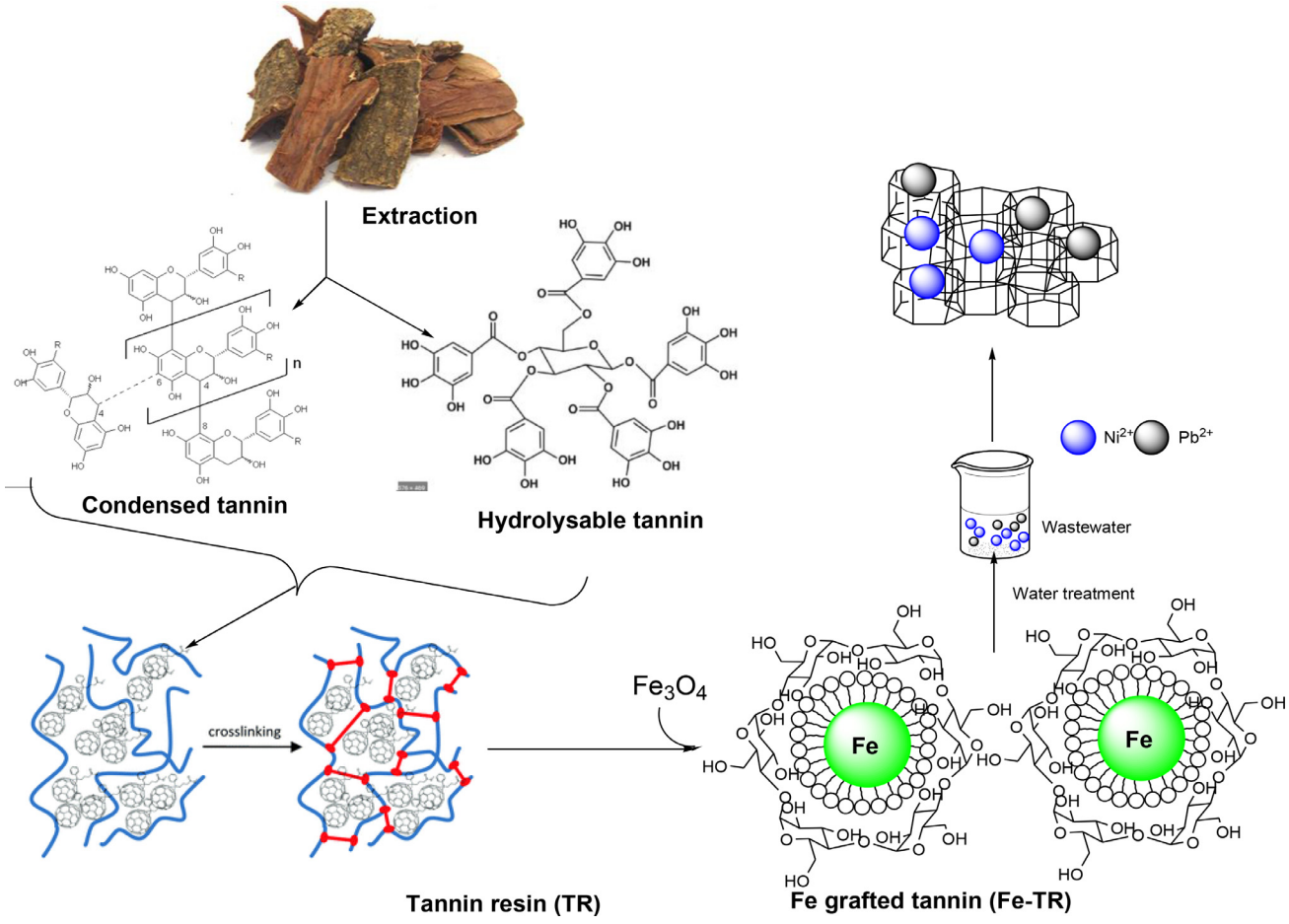


Fig. 2. Schematic diagram of experimental set-up.

was determined using inductively coupled plasma optical emission spectrometry (Perkin Elmer, Optima 5300 DV, MA). The sorbent loading at time (t) was evaluated using Eq. (1):

$$q = \frac{(C_i - C_f)V}{m} \quad (1)$$

Where q(mg/g): sorbent loading, V(L): volume of sorbent, m(g): the mass of sorbent, C_i and C_f: are the initial and final ion concentrations in ppm.

2.8. Evaluation of thermodynamic variables

The enthalpy (ΔH^o) and entropy (ΔS^o) changes were extrapolated from the slope and intercept of the plot of $\ln K_D$ vs 1/T (Eq. (2)); respectively, while the Gibbs free energy change (ΔG^o) was calculated from Eq. (3).

$$\ln K_D = -\frac{\Delta H^o}{RT} + \frac{\Delta S^o}{R} \quad (2)$$

$$\Delta G_o = -RT \ln K_D \quad (3)$$

Where, R: is the ideal gas constant (8.314 $J.mol^{-1}K^{-1}$), T: temperature (K), and K_D: distribution coefficient ($\ell \cdot mol^{-1}$).

2.10. Adsorption kinetics models

For the absorption kinetics studies; at optimal conditions, a mixture of 0.5 g and 50 mL of the adsorbent and 100 ppm metal ions; respectively, was stirred for 60 min at 150 rpm, filtered; followed by the determination of ion concentration. All analyses were done in triplicate and reported as mean. The fitness of the absorption kinetics was evaluated according to several models. The quadratic and linear forms of the Pseudo-first-order kinetic model are presented in Eqs. (4) and (5) (Jiang et al., 2015):

$$\frac{dq_t}{dt} = K_1(q_e - q_t) \quad (4)$$

$$\log(q_e - q_t) = \log q_e - \frac{K_1}{2.303}t \quad (5)$$

Where q_e and q_t: is the amount of ion adsorbed at equilibrium and time t in mg/g; respectively, t (min): time, and k_1 (1/min): rate constant. Using the linear plot of log ($q_e - q_t$) against t; the values of q_e and k_1 were extrapolated.

After the integration and application of the boundary conditions to the quadratic form of the Pseudo-Second-order kinetic model (6), the linear form of the model was expressed as Eq. (7). The rate constants k_2 (g/mg. min) and q_e, which were extrapolated from the slope and intercept of the plot of t/q_t against t was used to determine

$$\frac{dq_t}{dt} = K_2(q_e - q_t)^2 \quad (6)$$

$$\frac{t}{q_t} = \frac{1}{K_2 q_e^2} + \frac{1}{q_e}t \quad (7)$$

After applying the boundary conditions and integrating the Elovich kinetic model (8), the linear form was expressed as Eq. (9) according to Wu et al. (2009).

$$\frac{dq_t}{dt} = \alpha\, exp(-\beta q_t) \quad (8)$$

$$q_t = \frac{1}{\beta} \ln \alpha\beta + \frac{1}{\beta} \ln t \quad (9)$$

Where α is the initial ion sorption rate in mg/g. min and β is the chemisorption surface coverage and activation energy in mg/g.

The study by Hameed et al. (2008), expressed the intraparticle diffusion kinetic model as in Eq. (10). The linear plot of q_t against $\sqrt{t}$ was used to work out the constants C and K_{int}.

$$q_t = K_{int}\sqrt{t} + C \quad (10)$$

Where K_{int} is the intraparticle diffusion rate constant in mg/g.min$^{1/2}$ and C is the constant which provides an understanding of the thickness of the boundary layer.

2.11. Adsorption isotherms models

To determine the isotherm model that best describes the sorption process observed in this study; the following models were evaluated:

Langmuir isotherm is expressed in the linear form as in Eq. (11) (Chowdhury et al., 2011). The constants ($1/K_L$ and a_L/K_L), are extrapolated from the intercept and gradient of the plot of C_e/q_e versus C_e.

$$q_e = \frac{Q_O k_L C_e}{1 + K_L C_e} \quad (11)$$

Where q_e is the amount of adsorbate adsorbed per unit weight of the sorbent in mg/g, Q_o is the optimal monolayer coverage capacity in mg/g, b is the Langmuir isotherm constant in L/mg, and C_e is the amount in mg/L of the un-adsorbed ion at equilibrium.

Dubinin-Radushkevich (D-R) Adsorption Isotherm model is represented by the quadratic Eq. (12), with the linear form presented in Eq. (13) in the linear form (Acharya et al., 2009). The linear isotherm plot of $In\ q_e$ against $RT(1 + \frac{1}{C_e})$ gives $q_{m,}$ as the intercept.

$$\ln q_e = \ln q_s - K_D\varepsilon^2 \quad (12)$$

$$\text{with } \varepsilon = RT\left(1 + \frac{1}{C_e}\right) \quad (13)$$

Where K_D (mol^2/kJ^2): isotherm constant, and ε (J/mol K): isotherm gas constant

Temkin Adsorption Isotherm is linearly presented in Eq. (14) (Pursell et al., 2011). Therefore, the plot of q_e against $In\ C_e$ gives the intercept and slope; $In\ A_T$ and $RT/B_{T.;}$ respectively.

$$q_e = \frac{RT}{b_T} \ln A_T + \frac{RT}{b_T} \ln C_e \quad (14)$$

Where A_T, $b_{T,}$ and R are the Temkin binding (L/mg), Temkin isotherm(J/mol), and universal gas constants (J/mol K); respectively.

Freundlich Adsorption Isotherm is linearly expressed in Eq. (15) (Arshadi et al., 2015).

$$\log q_e = \log K_f + \frac{1}{n} \log C_e \quad (15)$$

Where K_f is the isotherm constant (mg/g) and n is the adsorption intensity. The constants (K_F and n) are extrapolated from the intercept and gradient of the plot of $In\ q_e$ versus $In\ C_e$.

3. Results and discussion

3.1. Quantification of tannin and characterisation of the sorbents

The extract yield and tannin content were determined to be 15.08 wt% and 124.8 mg/g gallic acid equivalent; respectively. The TR and Fe-TR were characterized by different analytical techniques, comparing their structural properties to detail the differences in their adsorption capacities.

Table 1
Elemental composition of the sorbent materials.

Elemental composition (%)	Tannin	TR	Fe-TR
Carbon	53.66	79.00	68.20
Hydrogen	3.08	5.67	5.06
Nitrogen	–	5.56	6.26
Oxygen	43.26	10.07	20.47

3.2. Functional group analysis

The surface functionality of the tannin extract, TR, and Fe-TR was analysed and the results presented (Fig. 3). A close examination of the tannin and TR spectra reveals vibrational peaks at 3200–3600 cm^{-1} indicative of –OH stretching frequency as reported in the study of Benavente-García et al. (2000). However, there is a slight reduction in the peak intensity of Fe-TR due to the surface formation of a metal-oxygen bond (Sangeetha and Philip, 2012). Besides, the peaks around 1500 – 1700, 1400 –1600, and 1000 - 1300 cm^{-1}correspond to the C=O, the aromatic –C=C– and phenolic stretching vibrations; respectively (Gupta et al., 2013).

As a consequence of the crosslinking of the tannin, an in-plane bending vibration around 1631–1697 cm^{-1} corresponding to the N–H was formed (Rozenberg et al., 2004). Furthermore, there was a shift in the C=O stretching vibration by 79 cm^{-1}; which was similar to the results observed in the studies of Bourtoom and Chinnan (2008); Hui et al. (2014); Sionkowska et al. (2014). After the interaction of the adsorbent metal ions, the observed OH (3200–3600 cm^{-1}) and C–O (1197 cm^{-1}) bands on the spectra of TR showed a reduced intensity (Figure S1(a) Supporting Information). Which are possible coordination sites for Ni^{2+} and Pb^{2+} (Di Rocco et al., 1997; Yruela, 2013). After metal-ion interaction, the spectra of Fe-TR showed a slight shift in peak position indicating a possible ion exchange (Figure S1(b) Supporting Information); similarly observed during the immobilization of ions using biochars derived from broiler litters (Uchimiya et al., 2010; Wang, 2012).

3.3. Elemental analysis

The conversion of tannin to TR impacts the elemental component of the adsorbent, causing an increase in the carbon content of TR due to a crosslinking reaction. Comparatively, the grafting of Fe into the TR to produce Fe-TR resulted in increase in% carbon and% nitrogen (Song et al., 2018) (Table 1).

3.4. Thermal properties

The response of tannin, tannin resin (TR), and iron-doped tannin resin (Fe-TR) to temperature variation between 30–900 °C is documented graphically in Fig. 4. According to Pintsuk et al. (2007), the region of importance lies between the melting and degradation points of any material. The materials showed variable moisture loss (weight%) of about 8.44%, 3.76%, and 7.39% for tannin, TR, and Fe-TR; respectively, at the same temperature (110 °C). Tannin showed the highest amount of moisture loss due to the high amount of hydroxyl group found within the crosslinked structure.

The high weight loss in tannin and Fe-TR corresponds to the loss of physically bound water molecules and the strong affinity of Fe for water; respectively, attributed to the presence of a-hydroxy group common to hydrolysable tannins (Danish et al., 2011).

At the second decomposition stage (degradation step), the tannin lost 40% of its weight attributed to the breakdown of the natural polyphenol backbone at around 230 °C (Bothara and Singh, 2012). However, the degradation step of the adsorbents occurred at a higher temperature of about 350 °C with 24.6% and 21.7% weight loss; respectively. Hence, degradation of TR and Fe-TR occurred at a higher temperature

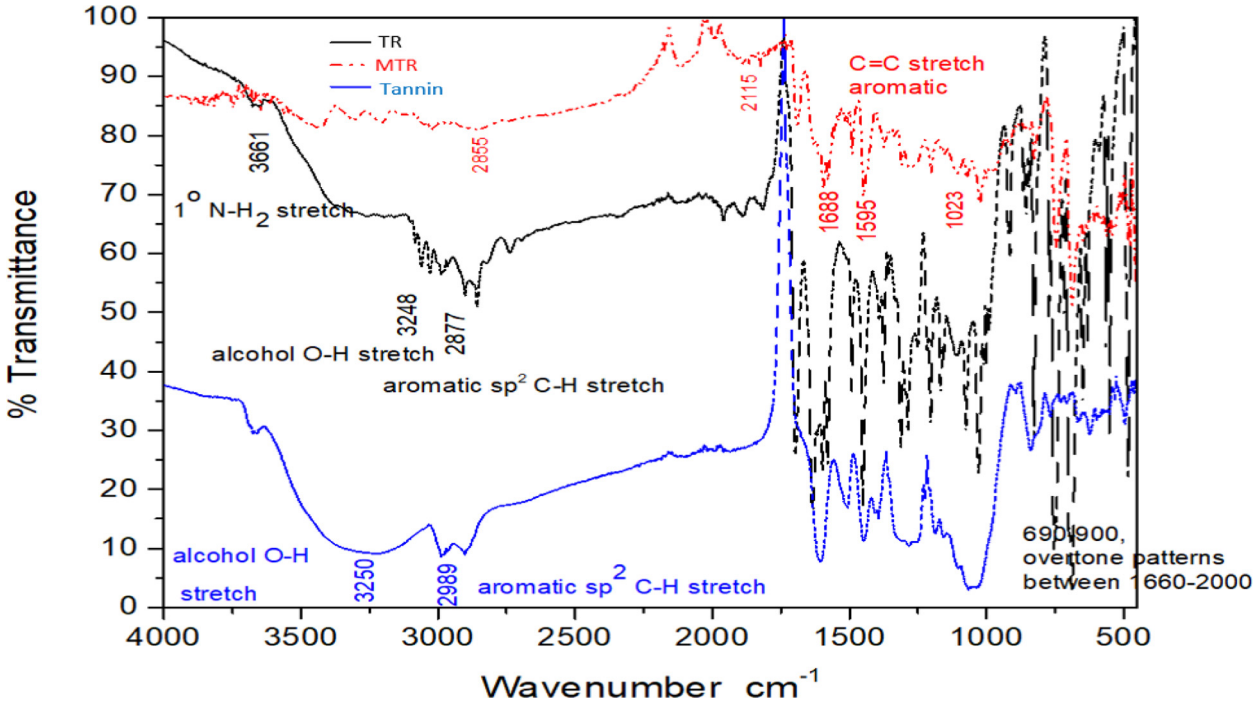


Fig. 3. FTIR spectra of the Tannin, TR and Fe-TR adsorbents.

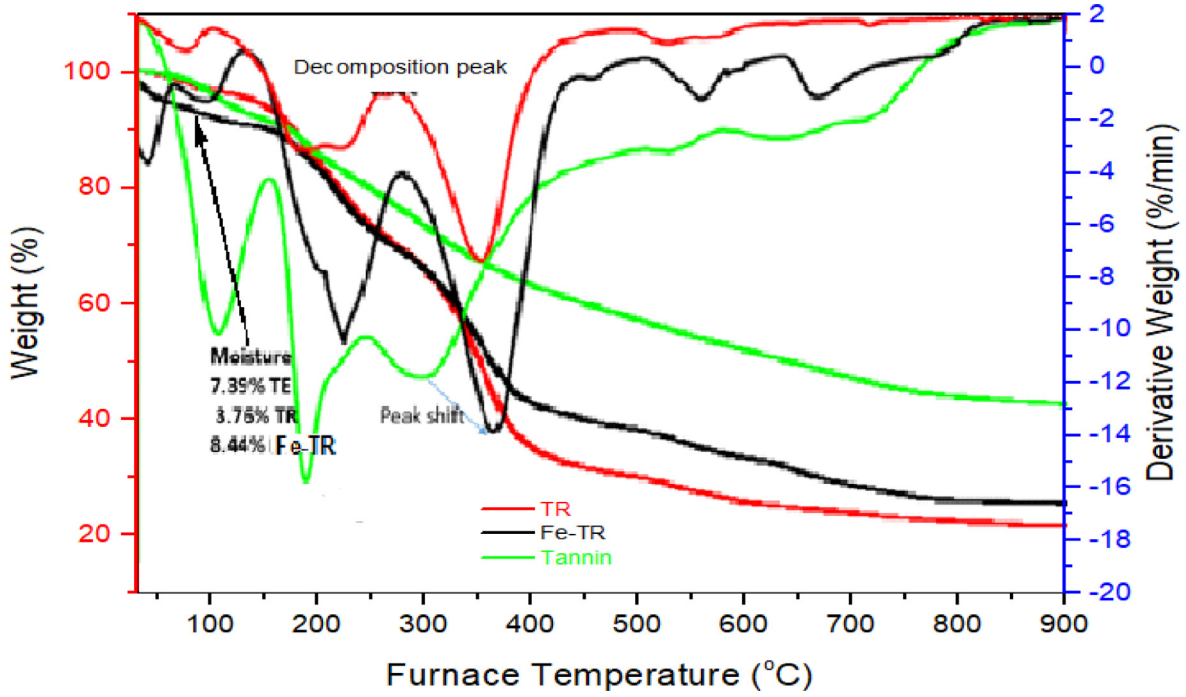


Fig. 4. Thermogram of the tannin and adsorbents (TR and Fe-TR) at 30 −900 °C.

compared to organic tannin obtained from *A. dealbata* bark with degradation at 257.77 °C (Lisperguer et al., 2016). Estimation of the ash generated after the complete combustion of TR, Fe-TR, and tannin is 46.5%, 72.4%, and 50.6%; respectively. Consequently, the large amount of ash formed by Fe-TR is due to the presence of Fe introduced during grafting.

3.5. X-Ray diffraction (XRD) evaluation of the materials

The obtained tannin and adsorbents were investigated by XRD instrument, equipped with Cu Kα radiation (1.54060 Å, 40 mA 45 kV) and the diffractograms are presented in Fig. 5. According to the XRD pattern of carbon material JCPDS number. 75–1621; and using the Scherrer equation the crystallite sizes of Fe-TR, TR and tannin were 11.94 nm, 5.93 nm and 12.38 nm; respectively. Tannin showed an amorphous characteristic (Atiqah et al., 2018). In contrast to the character of the adsorbents which appeared to have a crystalline structure. Besides, the Fe-TR showed a unique pattern similar to the diffraction lattice of Fe_3O_4 (Shyam et al., 2013).

There was no significant difference in the diffraction pattern of TR after the adsorption of Ni^{2+}, a possible sign of physical interaction (Fig-

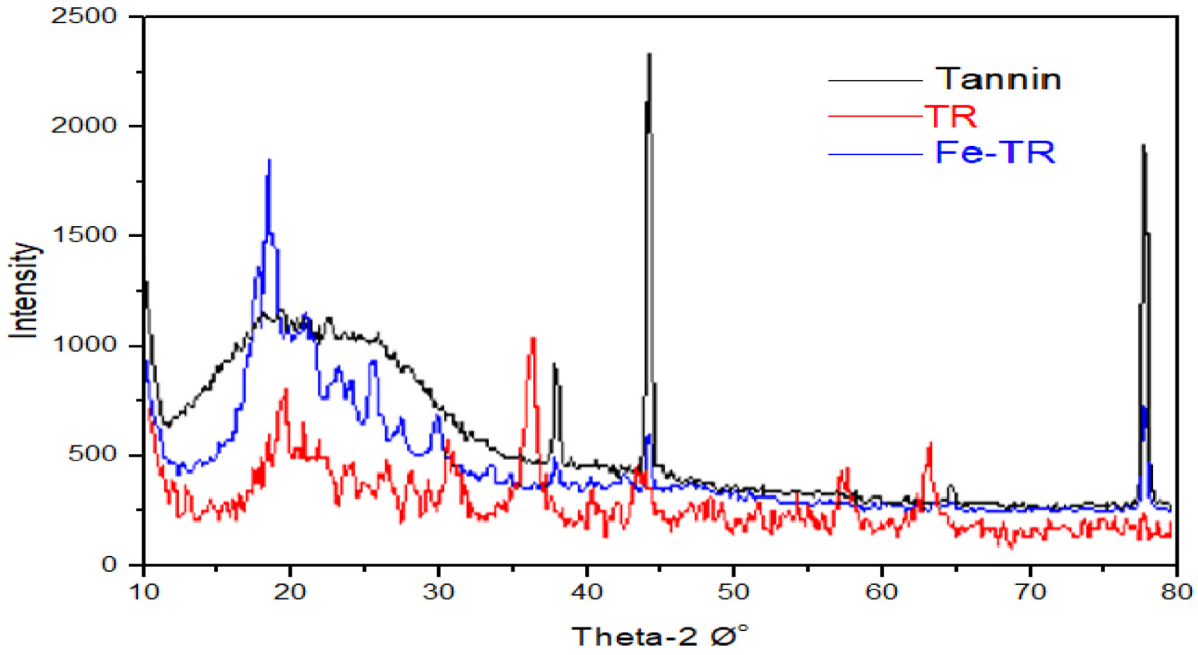


Fig. 5. XRD patterns of tannin, TR and Fe-TR.

Table 2
Adsorptive properties of the sorbents.

Analysed Parameters	TR	Fe-TR
Surface area (m^2/g)	1.6918	5.5386
Pore volume (cm^3/g)	0.0025	0.0330
Pore size (nm)	5.9696	23.8423

ure S2, Supporting Information). However, there is a slight alteration of the peak corresponding to 78° after the interaction of Pb^{2+} with TR; suggestive of a strong interactive force (Figure S3, Supporting Information). Largely, there was little disturbance on the diffraction pattern of Fe-TR after the adsorption of Ni^{2+}, although a prominent peak at 78° was introduced, which may be attributed to the chemical interaction with the surface of Ni^{2+} (Osuwa and Mgbaja, 2014).

Similarly, the interaction of Ni^{2+} and Pb^{2+} with Fe-TR caused no significant variation in the crystal structure; therefore, such a physical process is reversible (Liu et al., 2013).

3.6. Surface area and porosity structure of the adsorbents

Supporting information Figure S4 is the presentation of the nitrogen adsorption and desorption isotherm of the adsorbents. Both adsorbents showed a type II isotherm based on the isotherm classification by Rahman et al. (2006), indicative of unrestricted monolayer-multilayer adsorption with unlimited layer formation and no saturation limit (Abbatt et al., 2008). Although, Fe-TR showed more favourable adsorption of inert N_2 gas than TR, because, at a high relative pressure > 0.9, a steep increase indicates mesopore capillary condensation. The Brunauer Emmett Teller (BET) analysis showed a surface area increase, pore volume, and pore size for Fe-TR compared to TR (Table 2). A large surface area implies more adsorption surface and high adsorption capacity (Gupta et al., 2013).

3.7. Surface morphology and energy-dispersive X-ray (EDX) spectra of the materials

The micrography of tannin revealed a smooth, fine surface, with no distinct porous structure and large particle size with no defined dimensions. On the contrary, the Scanning Eelectron Microscopy (SEM) image of TR showed a well-defined morphology with a compact, crystalline, porous nature. More so, the morphology of Fe-TR showed a rough, heterogeneous, and irregular crevices (Fig. 6). After metal ion uptake, the morphological analysis of TR and Fe-TR indicated the formation of a whitish deposit and rough lump-like; respectively (Figure S5, Supporting Information).

Elemental mapping and EDX spectra of the adsorbents were carried out and reported as (Figures S6 and S7, Supporting Information). The colour mapping and spectra of the adsorbents revealed a significant amount of carbon underlying the adsorbents' organic nature. Besides, a large amount of organic carbon; a significant amount of iron was observed on the surface of Fe-TR. After the metal ion-adsorbent interaction, colour mapping confirms the random distribution of adsorbed Pb^{2+} and Ni^{2+} ions (Fig. 7), the spectra further confirm the presence of metal ion an evidence of ion interaction with the surface of the adsorbents.

3.8. Zero surface charge

The effect of solution pH on metal ion adsorption, the point of zero charge (pH_{PZC}) of TR, and Fe-TR were estimated (Fig. 8).

The pH_{PZC} for TR and Fe-TR was found to be 7.3 and 6.4; respectively.

According to Kumar et al. (2014), it was delineated that at pH below and above the pH_{PZC}; the net surface charge is positive and negative; respectively. By implication, the electrostatic attraction of cations is favoured by the negatively charged surfaces while anion interaction is favored on a positively charged surface. Hence, the negatively charged surface of TR and Fe-TR favours the adsorption of Pb^{2+} and Ni^{2+}. However, other interactions such as complexation and precipitation may lower the adsorption capacity of the metal ion, thereby delimiting the effect of surface charge (Salis et al., 2011).

3.9. Optimising the adsorption parameters

The removal of Pb^{2+} and Ni^{2+} ions showed pH-dependant sorption (Figure S8(a) Supporting Information), by implication the optimal adsorption capacities for Pb^{2+} and Ni^{2+} ions on TR and Fe-TR occurred at pH 4 and 6; respectively. These pHs are lower than their respective pH_{PZC}; hence, the observed interaction is not electrostatically

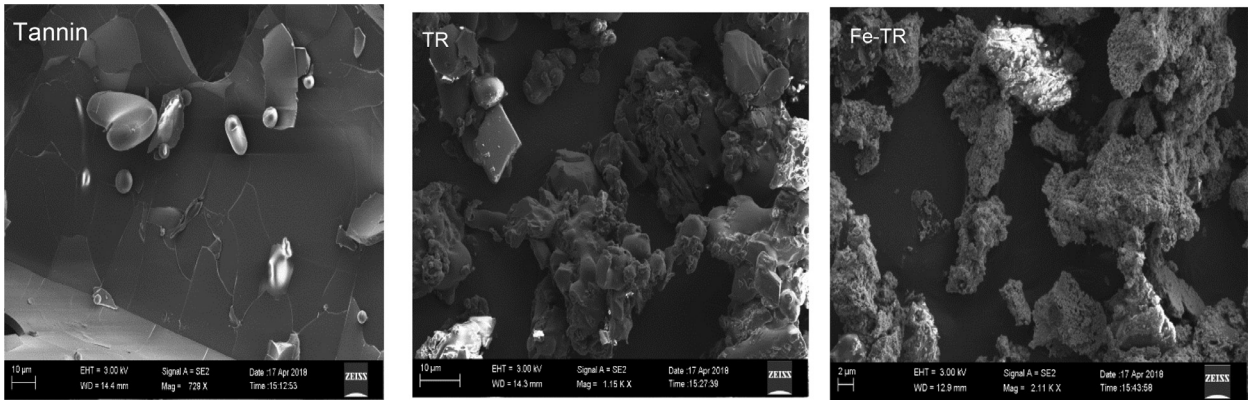


Fig. 6. Micrographs of Tannin, TR, and Fe-TR.

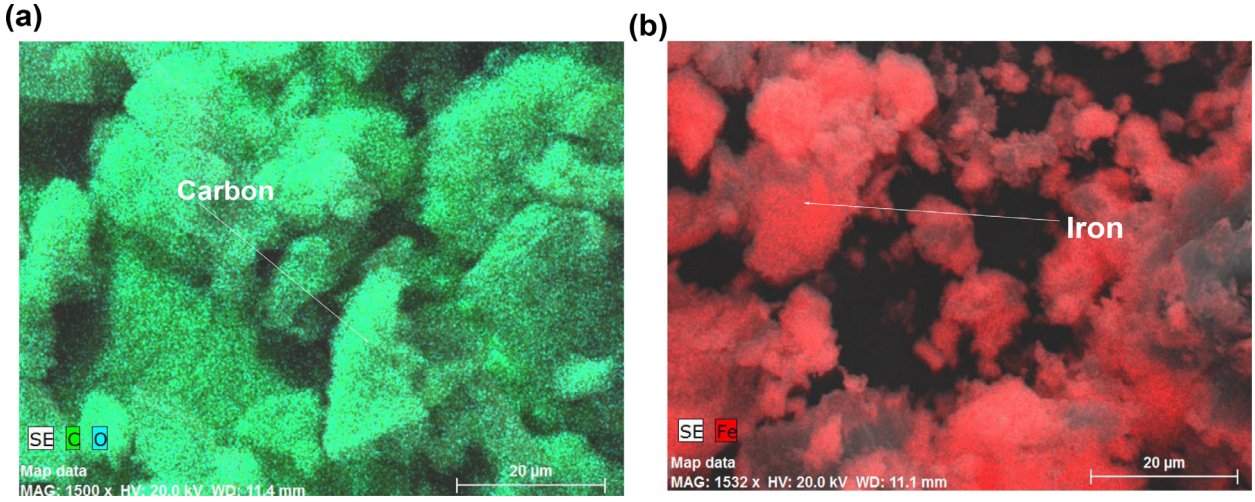


Fig. 7. EDX colour mapping of (a) TR and (b) Fe-TR.

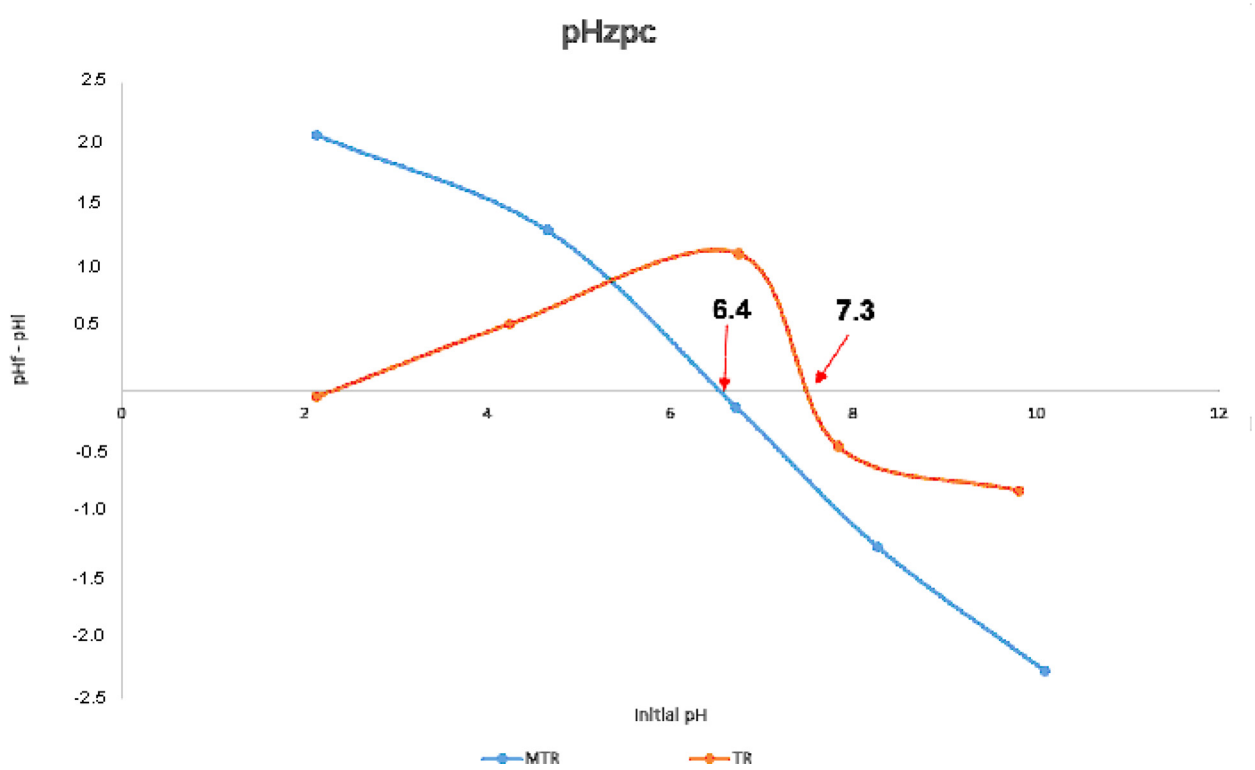


Fig. 8. Zero-point charge of TR and Fe-TR.

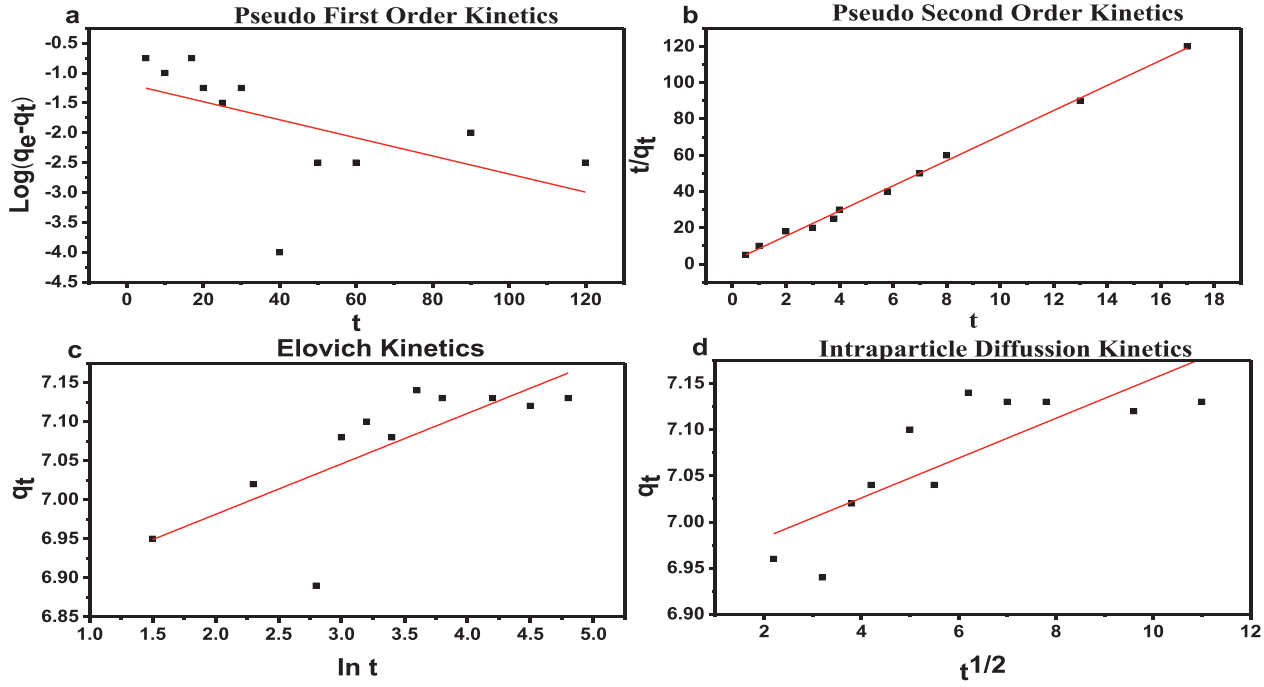


Fig. 9. Plots of (a) pseudo-second-order equation, (b) pseudo-first-order equation, (c) Elovich equation and(d) intra-particle diffusion equation; for the sorption of Pb^{2+} on TR.

Table 3
Thermodynamic parameters for the adsorption of Pb^{2+} and Ni^{2+} ions.

Adsorbents	ΔH^o (KJ/mol)	ΔS^o (J/(mol/K)	ΔG^o (KJ/mol) @298K
TR-Pb	67.29	233.32	−2.99
TR-Ni	26.51	57.66	9.56
Fe-TR-Pb	31.95	134.2	−8.15
Fe-TR-Ni	16.76	34.19	6.98

favourable. This confirms the influence of pH on the chelating capacity of the functional sites, the degree of speciation, and ionization of the ions (Singh et al., 2017). On the other hand, the concentration effect revealed that ion uptake by the adsorbents increased with metal ion concentration until an equilibrium concentration were established (Fig. S8(b), Supporting Information), indicating an unrestricted monolayer-multilayer adsorption process. This phenomenon perhaps is due to increased competition for the adsorption site as concentration increases with more interaction between the metal ions; subjugating all mass transfer restrictions between the aqueous and adsorbent surface leading to increased adsorption metal ions (Rezaei, 2016).

Thermal behaviour of the sorbents for ion uptake within the temperature range considered in this study showed that temperature does not significantly perturb the capacity of Pb^{2+} adsorption by both adsorbents. Although, there is a slight increase in the adsorption of Ni^{2+} with temperature (Fig. S9(a), Supporting Information). However, the contact time of the ions with the sorbents play a vital role in the removal efficiency of ions in solution (Fig. S9(b), Supporting Information); with equilibrium uptake of 10 min for Pb^{2+} compared to 60 min for Ni^{2+}. However, Fe-TR and TR adsorbed the highest amount of Pb^{2+} and Ni^{2+} in 10 min and 60 min; respectively. The amount of Pb^{2+} removed by Fe-TR from aqueous solution depends on the thermodynamic conditions; which favours the displacement of Pb^{2+} in solution by the surface Fe. Moreso, in the case of TR, the Ni^{2+} removal is not thermodynamically favoured; but proceeds via chelation by functional site on the surface. After metal ion uptake, the morphological analysis of Fe-TR indicated the formation of a rough lump-like surface compared to the rough, heterogeneous, and irregular crevices before adsorption.

Table 4
The kinetics model fitting parameters of Pb^{2+} and Ni^{2+} on the adsorbents.

Sorbents	Pseudo-First-Order equation			Pseudo-Second-Order equation			
	K_1 (min^{-1})	q_e (mg/g)	r^2	$q_{e,exp}$ (mg/g)	K_2 (g/mg min)	$q_{e,exp}$ (mg/g)	r^2
TR-Pb	0.0368	0.0759	0.3220	7.1390	0.6967	7.1480	0.9950
TR-Ni	0.0398	7.6966	0.5780	11.214	0.0025	14.556	0.9380
Fe-TR-Pb	0.0378	0.0959	0.2540	10.480	0.0413	10.787	0.9930
Fe-TR-Ni	−4.8358	0.0045	0.5780	7.0740	0.0019	10.917	0.6250

Sorbents	Elovich equation			Intraparticle-diffusion equation		
	α (mg/g min)	β (g/min)	r^2	K_{diff} (mg/g $min^{\frac{1}{2}}$)	C	r^2
TR-Pb	7.1258×10^{44}	15.456	0.7100	0.0212	6.9513	0.6020
TR-Ni	1.1098	0.2917	0.8810	1.1634	0.7733	0.8000
Fe-TR-Pb	59.985	0.7282	0.3830	0.3679	7.6318	0.2170
Fe-TR-Ni	0.6877	0.4762	0.9480	0.7036	0.5516	0.8410

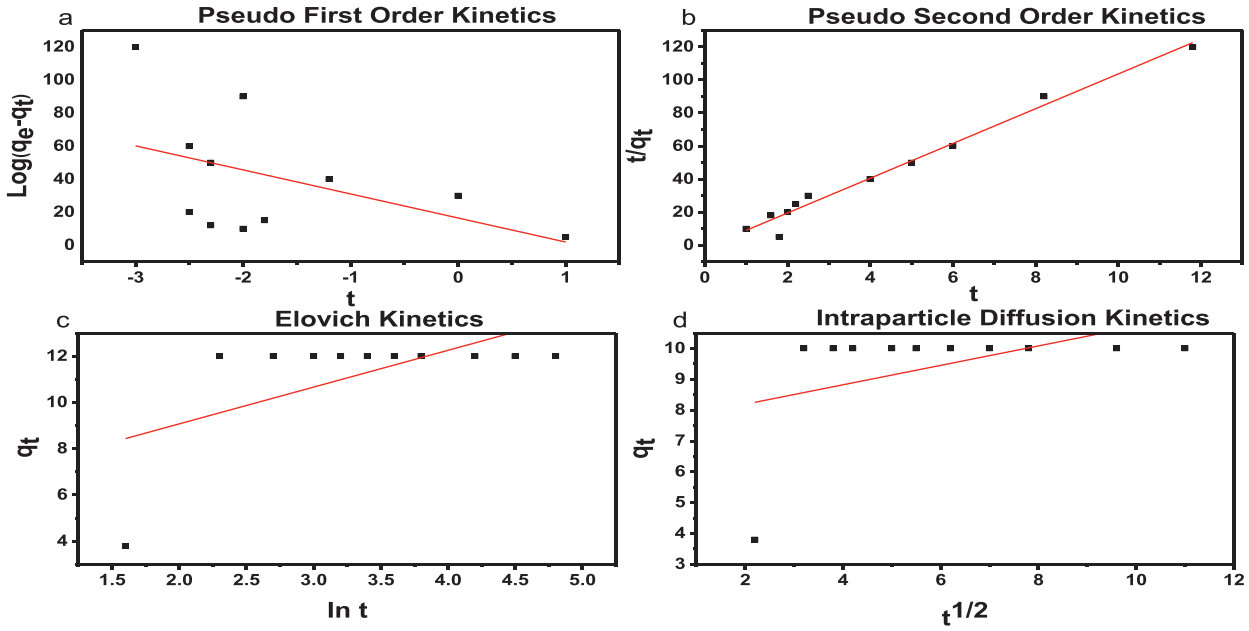


Fig. 10. Plots of (a) pseudo-second-order equation, (b) pseudo-first-order equation, (c) Elovich equation and (d) intra-particle diffusion equation; for the sorption of Ni^{2+} ions on TR.

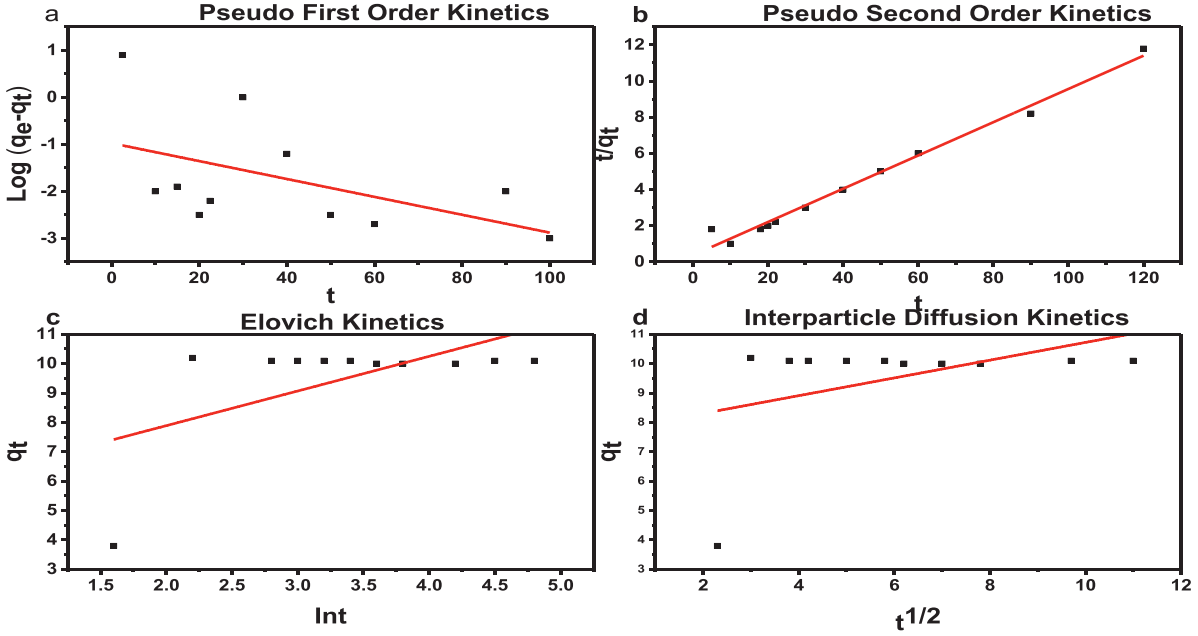


Fig. 11. Plots of (a) pseudo-second-order equation, (b) pseudo-first-order equation, (c) Elovich equation and(d) intra-particle diffusion equation; for the sorption of Pb^{2+} on Fe-TR.

Further, confirmed by the EDX colour mapping of the Fe-TR after ion uptake (Figure S6 and S7, Supporting Information).

3.10. Thermodynamic parameters

To further evaluate the thermodynamic parameter that governs the adsorption processes, the ΔG^o, ΔH^o, and ΔS^o) were determined and presented in Table 3.

A negative ΔG for the removal of Pb^{2+} by the adsorbents suggests a spontaneous and feasible process; which is in agreement with the rapid interaction of Pb^{2+} with the adsorbent. On the contrary, Ni^{2+} ions showed a slight uptake with temperature due to the positive ΔG (Lakshmi et al., 2009). The corresponding ΔH° values were endothermic for all adsorption processes with a positive ΔS^o indicating an irreversible process.

3.11. Predicting the kinetic and isotherm models for metal ion-adsorbent interaction

Table 4 shows the computed kinetic data for the adsorbent - ion interaction (Figs. 9 and 10). Adsorption of Pb^{2+} on both adsorbents showed a good relationship between the experimental and calculated equilibrium adsorption capacity (q_e) with correlation coefficient (r^2) > 0.99. Thus, the rate-controlling process is best depicted by the Pseudo-second-order kinetic model, which favours a chemisorption process (Aljeboree et al., 2017). Quite‘ the contrary, the adsorption data of Ni^{2+} on to the adsor-

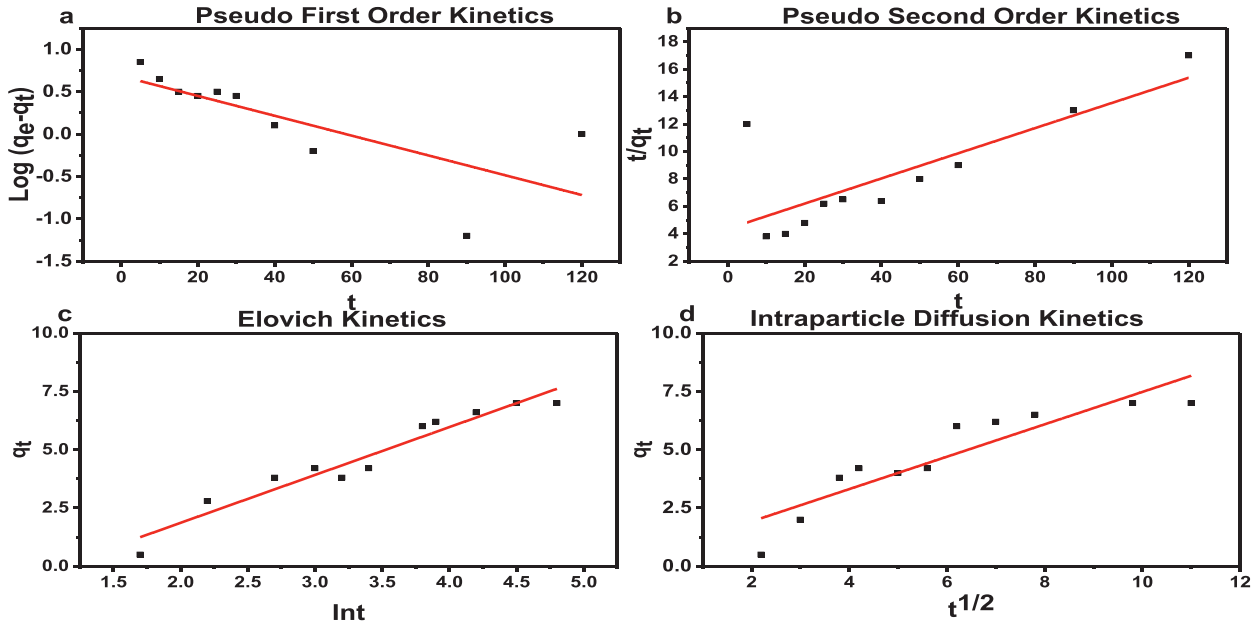


Fig. 12. Plots of (a) pseudo-second-order equation, (b) pseudo-first-order equation, (c) Elovich equation and(d) intra-particle diffusion equation; for the sorption of Ni^{2+} on Fe-TR.

Table 5
Equilibrium isotherm model parameters for adsorption of Pb^{2+} and Ni^{2+} ions.

Sorbents	Langmuir isotherm				Freundlich isotherm		
	Q_{max} (mg/g)	b (L/mg)	R_L	r^2	n	K_f (mg/g)	r^2
TR-Pb	40.650	0.0511	0.1636	0.9740	0.4819	4.6612	0.987
TR-Ni	13.763	1.0092	0.0098	0.9880	0.4476	12.797	0.969
Fe-TR-Pb	120.63	0.5964	0.0165	0.9390	1.5901	17.394	0.927
Fe-TR-Ni	110.74	2.5083	0.0040	0.9990	2.7586	14.067	0.910

Sorbents	Temkin isotherm			Dubimin-Radushkevich isotherm			
	b_T (J/mol)	A_T (l/mg)	r^2	Q_s (mg/g)	E (KJ/mol)	K_{DR} (mol/KJ)^2	r^2
TR-Pb	220.89	1.6224	0.9700	22.247	1.000	5.0×10^7	0.9870
TR-Ni	199.12	3.9353	0.8850	2.8137	2.2360	1.0×10^7	0.9730
Fe-TR-Pb	721.70	39.975	0.8540	11.457	4.0820	3.0×10^8	0.8770
Fe-TR-Ni	1218.7	346.57	0.8940	11.851	7.0710	1.0×10^8	0.9990

bents showed that there might be more than one kinetic model in play. The two plausible assumptions are the Elovich and intraparticle kinetics models, indicating adsorption on a heterogeneous surface (Largitte and Pasquier, 2016), as well as adsorbate. diffusing into the adsorbent's inner pores after being initially adsorbed on to the adsorbent's surface; respectively, this observation further supports multilayer adsorption. Furthermore, the boundary layer thicknesses (C) of the adsorbents are less than 1, suggesting that the rate-determining step is influenced by intraparticle diffusion and external mass transfer (Nethaji et al., 2013). This could have caused the prolonged time required for the adsorption of Ni^{2+} to reach equilibrium compared to Pb^{2+} ions.

To establish the optimal uptake capacity of the adsorbents for the ions, the data from the batch equilibrium investigations were fitted into a model to describe the adsorption process (Figs. 11 and 12). The parameters obtained by data fitting into the adsorption isotherm equations (Table 5); they revealed that four adsorption isotherms showed good correlations ($r^2 \geq 0.970$) for the ion-adsorbent interactions. Furthermore, the cement the possibility of monolayer and multilayer adsorption. The adsorption capacity (q_{max}) showed that the mass of Pb^{2+} ions adsorbed is greater than that of Ni^{2+}.

Furthermore, evaluation of the adsorption intensity (n), showed that n ⟨< 1 for the interaction of ions with TR and n > 1 for the interaction with Fe-TR, indicating a chemisorption and physisorption process; respectively (Afroze et al., 2016). According to Maji et al. (2007), it was inferred that a mean free energy less than 8 KJ/mol suggests a dominating physical process; although some degree of chemisorption was observed on TR. More so, the mean free energy for the ion - Fe-TR interaction implies that the adsorption taking place on the adsorbent surface is driven by a physical process. Hence, ion-adsorbate interactions in this study are reversible. The dimensionless separation parameter (R_L) ≤ 0.1636; this suggests that the processes were all endothermic and spontaneous process as further confirmed by the Temkin isotherm constant (B_T) (Pandey et al., 2015).

4. Conclusions

Based on our findings, *A. mearnsii* is a good feedstock for tannin, which can easily be crosslinked and Fe-grafted to produce the tannin traps for Pb^{2+} and Ni^{2+}. These tannin traps have good thermal stability, morphology, and surface chemistry. The crystallite sizes of the adsorbents were smaller compared to tannin with size of 12.38 nm; however, the% carbon and nitrogen were significantly higher. The Brunauer–Emmet–Teller analysis of the adsorbent showed that iron-grafting of tannin after crosslinking increases the surface area, pore

volume and pore size, which are prerequisites for enhanced adsorption. The interaction of Pb^{2+} ions with both adsorbents is spontaneous and governed by the pseudo-second-order kinetic, on the contrary, the nonspontaneous interaction of Ni^{2+} ions is better described by the intraparticle kinetics and Elovich models. The equilibrium isotherms revealed that the mechanism is a blend of both chemisorption and physisorption processes. The adsorbents showed a type II isotherm with adsorption capacities of 40.650 mg/g and 13.763 mg/g for Pb^{2+} and 120.63 mg/g and 110.74 for Ni^{2+} ion by TR and Fe-TR; respectively which is strongly pH-dependant. The sorption of metal ions on to Fe-TR gave a higher maximum adsorption capacity in comparison to their sorption on to TR. Finally, evaluating the effect of Fe-grafting on the performance of the TR, it can be concluded that grafted Fe causes a significant improvement in the adsorption performance of tannin-base adsorbent when used for water treatment.

Data availability

The data used to support this study are available within the manuscript.

Declaration of Competing Interest

The authors declare that they have no known competing financial interests or personal relationships that could have appeared to influence the work reported in this paper.

Funding Statement

The study did not receive any external funding; however, we wish to appreciate the Directorate of Research, Vaal University of Technology, South Africa.

Acknowledgments

We appreciate the Institute of Chemical and Biotechnology, Faculty of Applied and Computer Science Research, Vaal University of Technology, South Africa, for supporting the research.

Supplementary materials

Supplementary material associated with this article can be found, in the online version, at doi:10.1016/j.envc.2021.100058.

References

Abbatt, J.P.D., Bartels-Rausch, T., Ullerstam, M., Ye, T.J., 2008. Uptake of acetone, ethanol and benzene to snow and ice: effects of surface area and temperature. Environ. Res. Lett. 3. doi:10.1088/1748-9326/3/4/045008.

Acharya, J., Sahu, J.N., Mohanty, C.R., Meikap, B.C., 2009. Removal of lead (II) from wastewater by activated carbon developed from *Tamarind wood* by zinc chloride activation. Chem. Eng. J. 149, 249–262. doi:10.1016/j.cej.2008.11.035.

Adesola, N.A., Oyebamiji, J., Adebowale, S., 2006. Biosorption of lead ions from aqueous solution by maize leaf. Int. J. Phys. Sci. 1, 23–26.

Afroze, S., Sen, T.K., Ang, H.M., 2016. Adsorption removal of zinc (II) from aqueous phase by raw and base modified Eucalyptus sheathiana bark: kinetics, mechanism and equilibrium study. Process Saf. Environ. Prot. 102, 336–352. doi:10.1016/j.psep.2016.04.009.

Aljeboree, A.M., Alshirifi, A.N., Alkaim, A.F., 2017. Kinetics and equilibrium study for the adsorption of textile dyes on coconut shell activated carbon. Arab. J. Chem. 10, S3381–S3393. doi:10.1016/j.arabjc.2014.01.020.

Arshadi, M., Mehravar, M., Amiri, M.J., Faraji, A.R., 2015. Synthesis and adsorption characteristics of an heterogenized manganese nanoadsorbent towards methyl orange. J. Colloid Interface Sci. 440, 189–197. doi:10.1016/j.jcis.2014.10.053.

Atiqah, T.N., Tan, S.J., Foo, K.L., Supri, A.G., Al Bakri, A.M.M., Liew, Y.M., 2018. Effect of graphite loading on properties of polyaniline/graphite composites. Polym. Bull. 75, 209–220. doi:10.1007/s00289-017-2031-1.

Bakatula, E.N., Richard, D., Neculita, C.M., Zagury, G.J., 2018. Determination of point of zero charge of natural organic materials. Environ. Sci. Pollut. Res. doi:10.1007/s11356-017-1115-7.

Benavente-García, O., Castillo, J., Lorente, J., Ortuño, A., Del Rio, J.A., 2000. Antioxidant activity of phenolics extracted from Olea europaea L. leaves. Food Chem 68, 457–462. doi:10.1016/S0308-8146(99)00221-6.

Bothara, S.B., Singh, S., 2012. Thermal studies on natural polysaccharide. Asian Pac. J. Trop. Biomed. 2. doi:10.1016/S2221-1691(12)60356-6.

Bourtoom, T., Chinnan, M.S., 2008. Preparation and properties of rice starch-chitosan blend biodegradable film. LWT - Food Sci. Technol. 41, 1633–1641. doi:10.1016/j.lwt.2007.10.014.

Chowdhury, S., Mazumder, M.A.J., Al-Attas, O., Husain, T., 2016. Heavy metals in drinking water: occurrences, implications, and future needs in developing countries. Sci. Total Environ. 569–570, 476–488. doi:10.1016/j.scitotenv.2016.06.166.

Chowdhury, S., Mishra, R., Saha, P., Kushwaha, P., 2011. Adsorption thermodynamics, kinetics and isosteric heat of adsorption of malachite green onto chemically modified rice husk. Desalination 265, 159–168. doi:10.1016/j.desal.2010.07.047.

Danish, M., Hashim, R., Rafatullah, M., Sulaiman, O., Ahmad, A., Govind, 2011. Adsorption of Pb(II) Ions from Aqueous Solutions by Date Bead Carbon Activated with ZnCl2. Clean - Soil, Air, Water 39, 392–399. doi:10.1002/clen.201000185.

Di Rocco, M., Picco, P., Arslanian, A., Restagno, G., Perfumo, F., Buoncompagni, A., Gattorno, M., Borrone, C., 1997. Retinitis pigmentosa, hypopituitarism, nephronophthisis, and mild skeletal dysplasia (RHYNS): a new syndrome? Am. J. Med. Genet. doi:10.1002/(SICI)1096-8628(19971128)73:1<1::AID-AJMG1>3.0.CO;2-Y.

Ferreira Júnior, W.S., Siqueira, C.F.Q., De Albuquerque, U.P., 2012. Plant stem bark extractivism in the Northeast semiarid region of Brazil: a new aport to utilitarian redundancy model. Evidence-based Compl. Altern. Med. 2012, 1–11. doi:10.1155/2012/543207.

Fu, F., Wang, Q., 2011. Removal of heavy metal ions from wastewaters: a review. J. Environ. Manag. doi:10.1016/j.jenvman.2010.11.011.

Govind, P., Madhuri, S., 2014. Heavy metals causing toxicity in animals and fishes. Res. J. Anim. Res. J. Anim. Vet. Fish. Sci. Int. Sci. Congr. Assoc. 2, 17–23.

Gupta, V.K., Ali, I., Saleh, T.A., Siddiqui, M.N., Agarwal, S., 2013. Chromium removal from water by activated carbon developed from waste rubber tires. Environ. Sci. Pollut. Res. 20, 1261–1268. doi:10.1007/s11356-012-0950-9.

Hameed, B.H., Mahmoud, D.K., Ahmad, A.L., 2008. Equilibrium modeling and kinetic studies on the adsorption of basic dye by a low-cost adsorbent: coconut (Cocos nucifera) bunch waste. J. Hazard. Mater. 158, 65–72. doi:10.1016/j.jhazmat.2008.01.034.

Hui, B., Zhang, Y., Ye, L., 2014. Preparation of PVA hydrogel beads and adsorption mechanism for advanced phosphate removal. Chem. Eng. J. 235, 207–214. doi:10.1016/j.cej.2013.09.045.

Jiang, T., Liu, W., Mao, Y., Zhang, L., Cheng, J., Gong, M., Zhao, H., Dai, L., Zhang, S., Zhao, Q., 2015. Adsorption behavior of copper ions from aqueous solution onto graphene oxide-CdS composite. Chem. Eng. J. 259, 603–610. doi:10.1016/j.cej.2014.08.022.

Joseph, B., Sekomeng, J., 2017. New Pharmacophore from the Stem Bark Fractions of Acacia decurrens (Willd) an Invasive South Africa Tree. J. Appl. Chem. 2017, 1–28.

Kumar, E., Bhatnagar, A., Hogland, W., Marques, M., Sillanpää, M., 2014. Interaction of inorganic anions with iron-mineral adsorbents in aqueous media - a review. Adv. Colloid Interface Sci. doi:10.1016/j.cis.2013.10.026.

Lakshmi, U.R., Srivastava, V.C., Mall, I.D., Lataye, D.H., 2009. Rice husk ash as an effective adsorbent: evaluation of adsorptive characteristics for Indigo Carmine dye. J. Environ. Manag. 90, 710–720. doi:10.1016/j.jenvman.2008.01.002.

Largitte, L., Pasquier, R., 2016. A review of the kinetics adsorption models and their application to the adsorption of lead by an activated carbon. Chem. Eng. Res. Des. 109, 495–504. doi:10.1016/j.cherd.2016.02.006.

Lisperguer, J., Saravia, Y., Vergara, E., 2016. Structure and thermal behavior of tannins from Acacia dealbata bark and their reactivity toward formaldehyde. J. Chil. Chem. Soc. 61, 3188–3190. doi:10.4067/S0717-97072016000400007.

Liu, X., Song, Q., Tang, Y., Li, W., Xu, J., Wu, J., Wang, F., Brookes, P.C., 2013. Human health risk assessment of heavy metals in soil-vegetable system: a multi-medium analysis. Sci. Total Environ. 463–464, 530–540. doi:10.1016/j.scitotenv.2013.06.064.

Maji, S.K., Pal, A., Pal, T., Adak, A., 2007. Adsorption thermodynamics of arsenic on laterite soil. J. Surf. Sci. Technol. 23, 161–176.

Naima, R., Oumam, M., Hannache, H., Sesbou, A., Charrier, B., Pizzi, A., Charrier - El Bouhtoury, F., 2015. Comparison of the impact of different extraction methods on polyphenols yields and tannins extracted from Moroccan Acacia mollissima barks. Ind. Crops Prod. 70, 245–252. doi:10.1016/j.indcrop.2015.03.016.

Nethaji, S., Sivasamy, A., Mandal, A.B., 2013. Adsorption isotherms, kinetics and mechanism for the adsorption of cationic and anionic dyes onto carbonaceous particles prepared from Juglans regia shell biomass. Int. J. Environ. Sci. Technol. 10, 231–242. doi:10.1007/s13762-012-0112-0.

Ogata, T., Morisada, S., Oinuma, Y., Seida, Y., Nakano, Y., 2011. Preparation of adsorbent for phosphate recovery from aqueous solutions based on condensed tannin gel. J. Hazard. Mater. doi:10.1016/j.jhazmat.2011.05.073.

Okoli, B., Shilowa, P., Anyanwu, G., Modise, J., 2018. Removal of Pb2+from water by synthesized tannin resins from invasive South African Trees. Water (Switzerland) 10, 648. doi:10.3390/w10050648.

Osuwa, J.C., Mgbaja, E.C., 2014. Structural and Electrical Properties of Copper Sulfide (CuS) Thin Films doped with Mercury and Nickel impurities. IOSR J. Appl. Phys. 6, 28–31. doi:10.9790/4861-06532831.

Otieno, F.A.O., Ochieng, G.M.M., 2004. Water management tools as a means of averting a possible water scarcity in South Africa by the year 2025. Water SA 30, 668–672. doi:10.4314/wsa.v30i5.5181.

Pandey, P.K., Sharma, S.K., Sambi, S.S., 2015. Removal of lead(II) from waste water on zeolite-NaX. J. Environ. Chem. Eng. 3, 2604–2610. doi:10.1016/j.jece.2015.09.008.

Pintsuk, G., Kühnlein, W., Linke, J., Rödig, M., 2007. Investigation of tungsten and beryllium behaviour under short transient events. Fusion Eng. Des. 82, 1720–1729. doi:10.1016/j.fusengdes.2007.06.030.

Pursell, C.J., Hartshorn, H., Ward, T., Chandler, B.D., Boccuzzi, F., 2011. Application of the Temkin model to the adsorption of CO on gold. J. Phys. Chem. C 115, 23880–23892. doi:10.1021/jp207103z.

Rahman, M.A., Asadullah, M., Haque, M.M., Motin, M.A., Sultan, M.B., Azad, M.A.K., 2006. Preparation and characterization of activated charcoal as an adsorbent. J. Surf. Sci. Technol. 22, 133–140.

Rezaei, H., 2016. Biosorption of chromium by using Spirulina sp. Arab. J. Chem. 9, 846–853. doi:10.1016/j.arabjc.2013.11.008.

Roto, R., Yusran, Y., Kuncaka, A., 2016. Magnetic adsorbent of Fe 3 O 4 @SiO 2 core-shell nanoparticles modified with thiol group for chloroauric ion adsorption. Appl. Surf. Sci. 377, 30–36. doi:10.1016/j.apsusc.2016.03.099.

Rozenberg, M., Shoham, G., Reva, I., Fausto, R., 2004. Low temperature FTIR spectroscopy and hydrogen bonding in cytosine polycrystals. Spectrochim. Acta - Part A Mol. Biomol. Spectrosc. 60, 463–470. doi:10.1016/S1386-1425(03)00251-8.

Salis, A., Boström, M., Medda, L., Cugia, F., Barse, B., Parsons, D.F., Ninham, B.W., Monduzzi, M., 2011. Measurements and theoretical interpretation of points of zero charge/potential of BSA protein. Langmuir 27, 11597–11604. doi:10.1021/la2024605.

Sangeetha, J., Philip, J., 2012. The interaction, stability and response to an external stimulus of iron oxide nanoparticle-casein nanocomplexes. Colloids Surfaces A Physicochem. Eng. Asp. 406, 52–60. doi:10.1016/j.colsurfa.2012.04.049.

Shyam, R., Puri, J.K., Kaur, H., Amutha, R., Kapila, A., 2013. Single and binary adsorption of heavy metals on fly ash samples from aqueous solution. J. Mol. Liq. 178, 31–36. doi:10.1016/j.molliq.2012.10.031.

Singh, H., Chauhan, G., Jain, A.K., Sharma, S.K., 2017. Adsorptive potential of agricultural wastes for removal of dyes from aqueous solutions. J. Environ. Chem. Eng. 5, 122–135. doi:10.1016/j.jece.2016.11.030.

Sionkowska, A., Kaczmarek, B., Lewandowska, K., 2014. Characterisation of chitosan after cross-linking by tannic acid. Prog. Chem. Appl. Chitin its Deriv. 19, 135–138. doi:10.15259/PCACD.19.16.

Song, Y., Ma, R., Jiao, C., Hao, L., Wang, C., Wu, Q., Wang, Z., 2018. Magnetic mesoporous polymelamine-formaldehyde resin as an adsorbent for endocrine disrupting chemicals. Microchim. Acta 185. doi:10.1007/s00604-017-2593-5.

Stankovic, S., Kalaba, P., Stankovic, A.R., 2014. Biota as toxic metal indicators. Environ. Chem. Lett. doi:10.1007/s10311-013-0430-6.

Uchimiya, M., Lima, I.M., Thomas Klasson, K., Chang, S., Wartelle, L.H., Rodgers, J.E., 2010. Immobilization of heavy metal ions (Cu II, Cd II, Ni II, and Pb II) by broiler litter-derived biochars in water and soil. J. Agric. Food Chem. 58, 5538–5544. doi:10.1021/jf9044217.

Valavanidis, A., Vlachogianni, T., 2010. Metal pollution in ecosystems. Ecotoxicology studies and risk assessment in the marine environment. Sci. Adv. Environ. Toxicol. Ecotoxicol. 1–9.

Verma, R., 2017. Heavy metal water pollution- A case study Heavy metal water pollution-a case study. Recent Res. Sci. Technol. 5, 98–99.

Wang, X., 2012. Nanomaterials as sorbents to remove heavy metal ions in wastewater treatment. J. Environ. Anal. Toxicol. 02. doi:10.4172/2161-0525.1000154.

Wasi, S., Tabrez, S., Ahmad, M., 2013. Toxicological effects of major environmental pollutants: an overview. Environ. Monit. Assess. doi:10.1007/s10661-012-2732-8.

Lee, Wonsuk, Lee, Kangchan, Lee, Seungyun, 2008. Intermediary based architecture for mobile Web services. J. Am. Sci. doi:10.1109/icact.2006.206381, pp. 6 pp. –1978..

Wu, F.C., Tseng, R.L., Juang, R.S., 2009. Characteristics of Elovich equation used for the analysis of adsorption kinetics in dye-chitosan systems. Chem. Eng. J. 150, 366–373. doi:10.1016/j.cej.2009.01.014.

Xiao, Z., Tian, G., Zhang, J., Li, S., Song, Y., Zhai, S., An, Q., 2012. Pb(II) removal of Fe3O4@SiO2–NH2 core–shell nanomaterials prepared via a controllable sol–gel process. Chem. Eng. J. 215–216, 461–471. doi:10.1016/j.cej.2012.11.043.

Yruela, I., 2013. Transition metals in plant photosynthesis. Metallomics doi:10.1039/c3mt00086a.